

F2008-SC-001

INVESTIGATION OF CAVITATION IN A LARGE-SCALE TRANSPARENT NOZZLE

¹Stanley, Cameron*, ¹Rosengarten, Gary, ¹Milton, Brian, ¹Barber, Tracie
¹University of New South Wales, Australia

KEYWORDS – Cavitation, Nozzle, PIV, Spray, Break-up

ABSTRACT

Cavitation through the nozzle of a diesel fuel injector is known to have a dramatic influence on the liquid jet atomisation. In order to investigate the relationship between cavitation cavity length and turbulence, high speed visualisation and particle image velocimetry (PIV) measurements have been conducted. Compressed air was used to drive filtered tap water through a large-scale, sharp-edged, acrylic nozzle with an L/d ratio of 5. Cavitation regimes ranging from incipient cavitation to supercavitation were explored and as a result the following conclusions were obtained: (1) Shed cavitation bubbles convected through the nozzle exit plane for the supercavitation regime have a dramatic influence on the liquid jet structure and aid the aerodynamic shear break-up of the jet. (2) Turbulent Kinetic Energy (TKE) was shown to be strongly linked to the cavitation cavity length and less dependent on Reynolds number.

INTRODUCTION

The atomisation of diesel fuel is known to be highly dependent on the internal flow through the injector nozzle. The first attempts to elucidate the effects of the nozzle on the fuel break-up process were by Bergwerk[1]. He found that cavitation, resulting from the high velocities, had a dramatic influence on the appearance of the fuel jet emerging from realistically sized nozzles. These findings were further supported by an extensive study of nozzle flows conducted by Reitz and Bracco[2]. Since these early studies, cavitation effects within nozzles have been studied extensively using both real sized nozzles [3-5] and scaled up transparent nozzles [6-8]. In fact, the large majority of experimental studies have used scaled-up nozzles, given the difficulties associated with flow measurements and visualisation of the phenomenon that result from the small physical dimensions and high pressures in real sized nozzles.

Despite the difficulties associated with scaling cavitation [9, 10], large scale experiments offer greater accessibility to visualise the cavitation and allow the effects of cavitation on general nozzle flow and spray characteristics to be easily described [3, 7]. Typically, dynamic flow similarity has been used to correlate large scale cavitation studies to realistic engine operating conditions with very few studies matching both Reynolds number and Cavitation number simultaneously as achieved by Soteriou et al. [3].

A number of researchers have used high speed visualisation to investigate cavitation within nozzles. Kim et al. [6] seeded water with aluminium oxide (Al_2O_3) tracer particles and used a flash lamp and high speed camera to visualise the internal flow structure of a 10 times scaled up injector nozzle. Badock et al. [11] used a laser light sheet to visualize the cavitation present in a real sized injector nozzle and found that even when the cavitation films extended to the

exit plane of the nozzle, the jet retained a solid liquid core. Soteriou et al. [12] used a laser light sheet to study the onset and development of cavitation structure in a large-scale nozzle. Velocity profiles were also measured using the Laser Doppler Velocimetry (LDV) technique for non-cavitating conditions.

Recently Sou et al. [13, 14] used LDV to measure the relationship between cavitation and turbulence levels in a two-dimensional, large-scale, nozzle orifice. Investigating cavitation regimes from developing to supercavitating flows, the authors showed a link between a lateral component of velocity and the enhancement in jet atomisation. Their study also demonstrated a relationship between the cavity length and spray angle of the issuing jet for both filtered tap water and light oil.

The current work investigates the relationship between cavitation cavity length and turbulence within an axisymmetric large-scale acrylic nozzle using the PIV technique and high speed photography. Cavitation number has been defined here as $\sigma = (P_u - P_v) / (P_u - P_d)$, where P_u is the upstream pressure, P_v is the vapour pressure and P_d is the nozzle outlet pressure (atmospheric for these experiments). The conditions investigated here do not represent realistic engine conditions in relation to either Reynolds number or Cavitation number. However, they do cover the span of cavitation structures from incipient to supercavitation for this particular nozzle geometry.

EXPERIMENTAL SETUP

A schematic of the system used for the current work is shown in Fig 1. Tap water used for the experiments was passed through a sediment removal filter, removing particles greater than $5\mu\text{m}$ and discharged through the nozzle into atmospheric air. No direct measures were employed to control the dissolved gas content of the water used for the experiments outlined in this work or to determine the nuclei distribution present. The nozzle used for the experiments was machined from acrylic and polished to an optically clear finish. Dimensions of the nozzle and the pre-nozzle chamber are shown in Fig 2. To minimise refraction of the light passing from the internal nozzle to the camera, a flat surface was machined and polished on the exterior of the nozzle at four positions separated at 90° intervals.

High pressure air was used to drive the nozzle discharge with a pressure regulator to ensure the pressure supply remained constant throughout the injection process. Maximum fluctuations were measured and controlled to within 5% of the mean driving pressure for all cases. Approximately 6 L of water was placed into the supply tank for each discharge before isolating the water line. The tank was then charged to a set pressure, with the remaining 5 L of space acting as a pressure buffer to the air supply from the compressor during the discharge. Pressure on the upstream side of the nozzle was measured using a piezo-electric pressure transducer (Honeywell - 20bar max) with a response time of 1ms and a linearity of $\pm 1\%$. Water temperature throughout the experiments was measured using a t-type thermocouple fixed in the top of the pre-nozzle chamber, accurate to $\pm 0.1^\circ\text{C}$. In order to ensure the system was primed before the start of a discharge and all vapour had been removed from the piping between the supply tank and the nozzle, a bleed valve placed in the top of the pre-nozzle chamber.

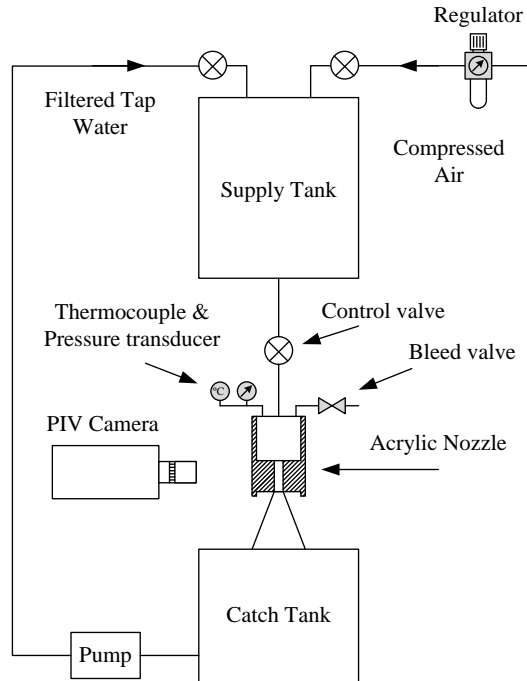


Fig. 1. Schematic of cavitation rig.

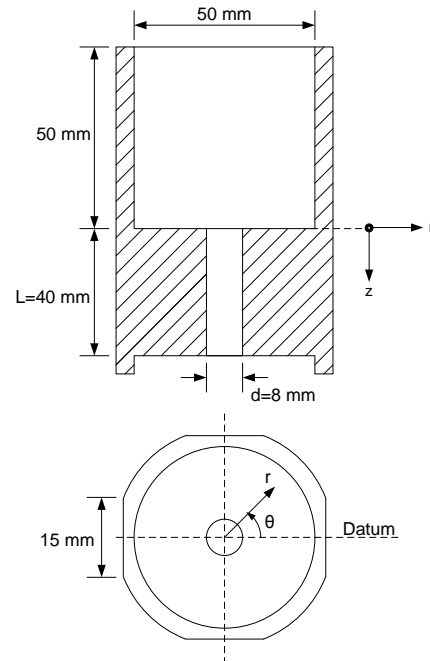


Fig. 2. Nozzle cross-section and top-view.

High Speed Visualisation

The evolution of the cavitation through the nozzle and the discharging jet was visualized using a high speed digital camera (Photron Ultima APX-RS) at 20,000 frames per second with a Nikon Nikkor lens ($f = 35\text{mm}$). Lighting for the camera was provided by two 300 W halogen lamps situated adjacent to the camera. An external trigger initiated image acquisition once the water discharge had reached steady state. In order to ensure that temporal and spatial changes in cavity structure were captured, 3 sets of 100 images were acquired separated by approximately 750ms, during each discharge. This process was repeated for 10 discharges at 4 different supply tank driving pressures, P_t . The position of the high speed camera was the same as for the PIV camera (shown in Fig 1.)

Cavity length, L_{cav} , was measured by image processing of the acquired images using visual recognition of the mean reattachment region. From each set of 100 images acquired, 10 representative equally spaced images were chosen and used to calculate a mean cavity length. This process was repeated for each of the 10 discharges, resulting in a mean length for each cavitation number calculated from 300 images.

PIV System

Instantaneous velocity fields downstream of the cavitation reattachment region were acquired using a high-speed CCD camera (SensiCam SuperVGA). The CCD camera has a total of 1280×1024 pixels each with a cell size of $6.7\mu\text{m} \times 6.7\mu\text{m}$. The field of view was illuminated by a double-pulsed Nd:YAG laser (532nm) having 120mJ of energy per pulse and a pulse-width of 5ns. A TEC telecentric Computar lens ($f = 55\text{mm}$) was used to visualise the flow giving a spatial resolution of $13.4\mu\text{m}/\text{pixel}$. Polyamide particles with an average diameter of $20\mu\text{m}$ were used to seed the water during PIV measurements. The timing of the laser system and image acquisition was controlled by the PIV synchroniser (Intelligent Laser Applications)

using the PIVsync software. The maximum repetition rate of the system is limited by the readout time of the camera and limited to 4 Hz (8fps). The time separation between the double pulses, Δt_p , was typically $6\mu s$ but was adjusted to ensure optimal particle displacement.

A two-frame direct cross-correlation method was used to determine the velocity fields from the acquired image pairs using VidPIV software (Intelligent Laser Applications). Initial interrogation windows of 64×64 pixels (50% overlap) were applied for a first-pass interrogation. Both global and local filter were applied before a second-pass, 32×32 pixels (50% overlap), adaptive cross-correlation was applied. Further global and local filtering was applied with erroneous vectors replaced with interpolated data from surrounding vectors (<6%). In order to ensure statistically independent sampling a total of 100 image pairs were collected from different injections and ensemble averaged for each driving pressure condition.

RESULTS & DISCUSSION

The following table summarises the conditions for each of the discharges measured.

Case	P_t (kPa)	P_u (kPa)	σ	L_{cav} (mm)	L_{cav}^* (L_{cav}/L)	Re ($\rho U d/\mu$)
1	400	251.7	1.66	5.13	0.13	1.07×10^5
2	500	269.5	1.59	8.07	0.20	1.31×10^5
3	600	286.7	1.53	25.51	0.66	1.41×10^5
4	700	306.9	1.48	39.20	0.98	$1.74 \times 10^{5*}$

Table 1. Summary of test conditions. *Re for case 4 was determined by image processing in a similar fashion to L_{cav} .

High Speed Visualisation

Typical examples of the cavitation structure revealed using the high speed digital camera are shown in Fig 3. It can be seen from these images that the cavitation spans from incipient cavitation ($\sigma = 1.66$) through to supercavitation ($\sigma = 1.48$).

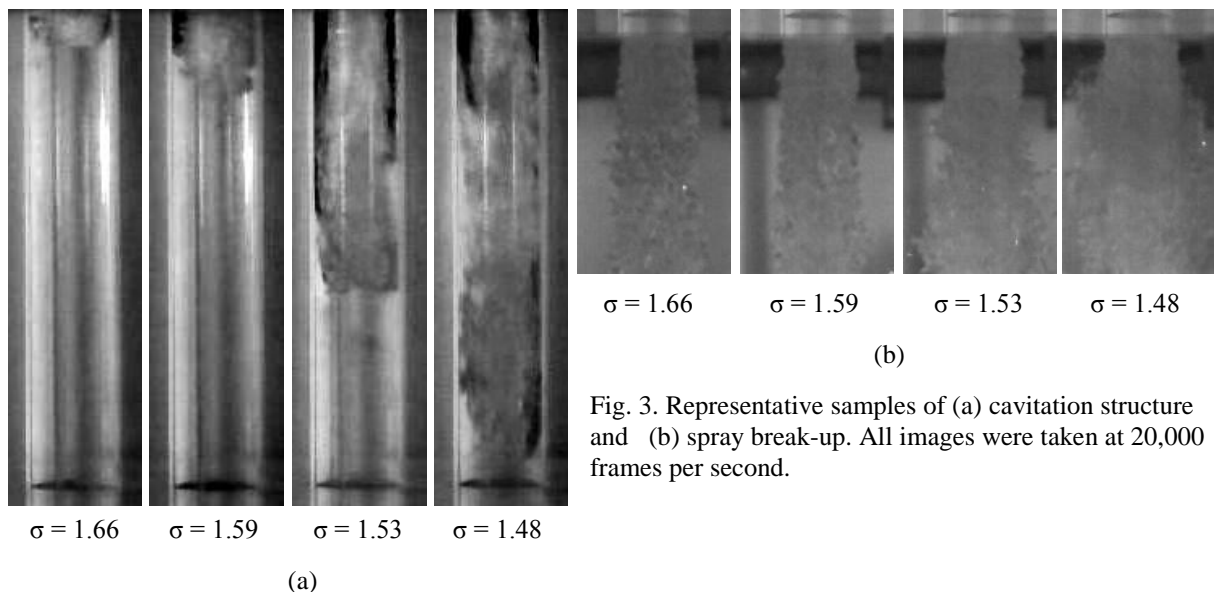


Fig. 3. Representative samples of (a) cavitation structure and (b) spray break-up. All images were taken at 20,000 frames per second.

The cavity surface appears rough and unsteady for each of the cases. It can be seen in the images from Fig. 3(a) that the cavity length for the lowest two driving pressures ($\sigma = 1.66$ and $\sigma = 1.59$) are quite similar when compared to the higher pressure cases ($\sigma = 1.53$ and $\sigma = 1.48$). The cavity for the $\sigma = 1.48$ (supercavitation) can be seen to extend all the way from the nozzle inlet to the exit. When the spray structures for this case, Fig. 3(b), is compared to the higher σ cases, it can be seen that the spray exiting the nozzle is significantly more divergent and bushier in appearance. From general observation, there is a definite increase in the spray angle the closer the cavitation reattachment is to the nozzle exit.

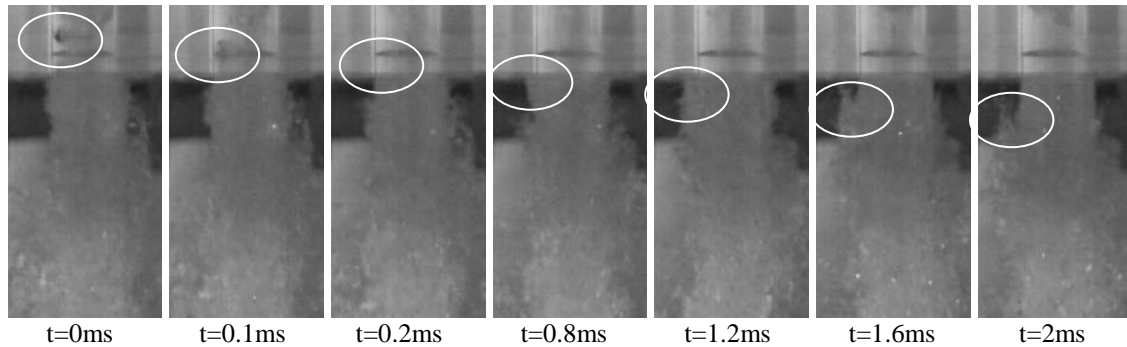


Fig. 4. Sequential cavitation images showing the shedding cavitations influence on spray structure ($\sigma = 1.48$)

The sequence of images in Fig. 4 are taken from the highest driving pressure condition ($\sigma = 1.48$) and demonstrate the huge influence that the shedding cavitation clouds have on the spray structure. The first image shows a cloud structure beginning to break away from the main cavity. It should also be noted that the section of the jet below the nozzle is ruffled but intact for at least 2 nozzle diameters downstream. By the second image, the cloud is travelling through the nozzle hole as a separate flow structure. By the time of the fourth image, the convected bubble cloud has caused the jet to diverge explosively. The following three images show the progression of this divergent liquid blast. It can be seen that this divergent blast is then much more exposed to aerodynamic shear which tears it apart as it begins to form ligaments of fluid and atomize. These findings agree well with Ganippa et al [15] who proposed it was these shedding vapour clouds that were responsible for the creation of asymmetric jets in cross-flow nozzles.

Normalised cavity lengths, $L_{cav}^* = L_{cav}/L$, were determined by post-processing of the acquired images for a series of 10 injections at each of the 4 injection pressures. The pressure recorded by the transducer was then analysed and the mean cavitation number for each injection determined. The results for this can be seen in Fig. 5. Due to the 3 dimensional spatial distribution of the cavity structure within the nozzle and the difficulty in defining the exact location of the reattachment point, a representative mean length was chosen visually for each image. The selection of this point attempted to take into consideration the objective of determining this parameter for use in a correlation. Hence it was chosen to represent a value that encompassed the overall flow structure for that particular instant in time.

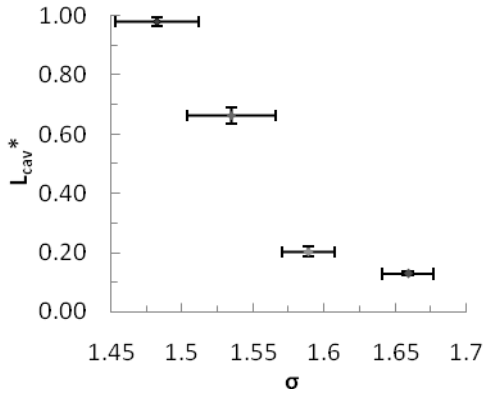


Fig. 5. Normalised cavity length, L_{cav}^* plotted against cavitation number, σ . Error bars indicate 95% confidence intervals.

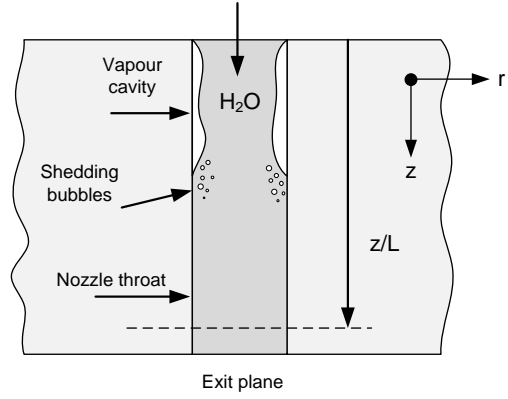


Fig. 6. Location of plane used for comparison of TKE from PIV results ($z/L = 0.9125$).

PIV results

The axial length of the interrogation volume used during PIV measurements varied for each of the driving pressures in order to maximise the region of interest whilst avoiding damage to the camera from light reflecting off the shedding bubbles. For the two lowest driving pressure cases ($\sigma = 1.66$, $\sigma = 1.59$), the interrogation area covered the entire camera field of view. For both these cases, the normalised mean cavity length, $L_{cav}^* \leq 0.2$, whereas for the higher injection pressures ($\sigma = 1.53$, $\sigma = 1.48$), the cavity length was much further towards the outlet of the nozzle. In order to overcome this, the laser light sheet was blocked to the upper $\frac{3}{4}$ of the nozzle and the interrogation volume moved towards the nozzle exit. Despite this, as the $L_{cav}^* \approx 1$ for the $\sigma = 1.49$ case, no PIV measurements were possible. The effect of the seeding particles on the cavitation has not been directly investigated here but would be expected to slightly increase the L_{cav}^* for these cases.

Turbulent Kinetic Energy

Subdividing the instantaneous velocity vector into a mean and fluctuating component

$$U_i(\vec{x}, t) = \overline{U}_i(\vec{x}) + u_i(\vec{x}, t)$$

where $\overline{U}_i(\vec{x})$ is the time average velocity and $\overline{u_i^2}$ is the variance of velocity. Because the nozzle we were measuring was axisymmetric we have used a cylindrical polar coordinate system

$$\vec{x} = (x_1, x_2, x_3) = (r, \theta, z); \vec{u} = (u_1, u_2, u_3)$$

In this study measurements were taken in a single bisecting plane and only radial (r) and axial (z) velocities were measured. As no information relating to the polar velocity component was measured the Turbulent Kinetic Energy will be defined for this work as:

$$TKE = \frac{1}{2} (\overline{u_r^2} + \overline{u_z^2})$$

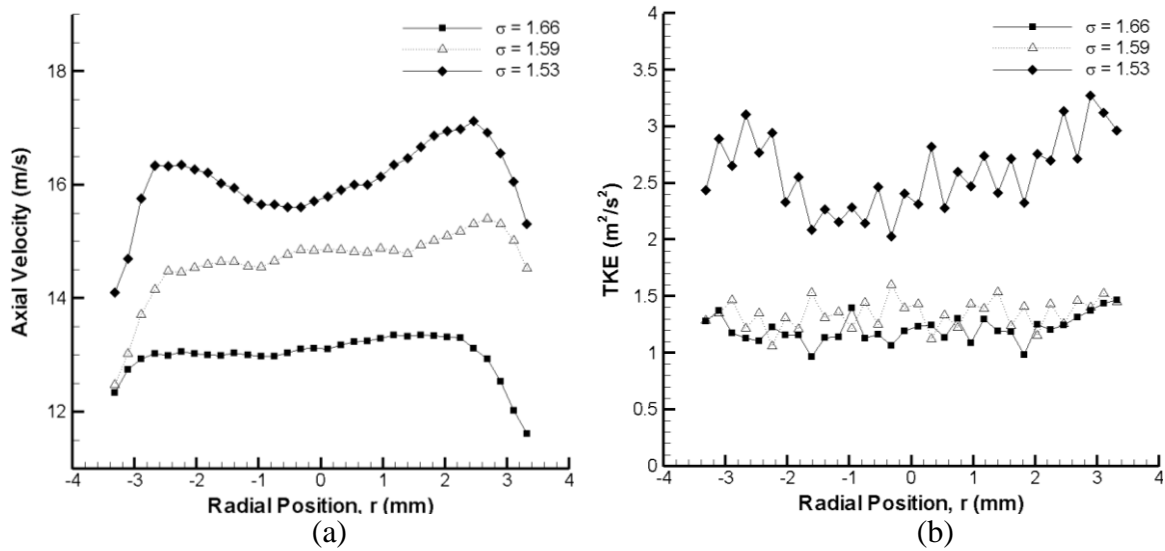


Fig. 7. Profiles at axial position $z/L = 0.9125$ of (a) axial velocity and (b) TKE

Plots of velocity near the nozzle exit ($z/L = 0.9125$) in Fig. 7(a) show a slight increase in axial velocity towards the right side of the nozzle. As this trend is consistent across the different driving pressures, it indicates that the cause lies in a slight geometrical asymmetry which acts as a cavitation nucleation site and increases the cavitation length on the right hand side. As a result, reattachment of the cavity will occur slightly further down the nozzle. Due to conservation of momentum, the presence of bubbles results in higher localised liquid velocities. This perhaps also explains the increasing gradient in this velocity asymmetry with a decrease in σ . As the L_{cav}^* increases, the distance between the shed bubble collapse and the measurement location becomes smaller. As such, the influence of the localised velocity increase to compensate for the reduction in density is more apparent. This effect could also account for the irregular shape of the velocity profile for the $\sigma = 1.53$ case. The velocity profile can be seen to have two peaks at a radial location of approximately ± 2.6 mm. These locations would correspond well to the expected radial location of the shed bubble clouds which are suggested as the cause for the increase in axial velocity. This effect would be expected to be much more pronounced for this case than the lower driving pressure cases as there is a much shorter distance from the measurement plane to the cavity reattachment region.

It can be seen from Fig. 7(b) that both of the lower driving pressure discharges ($\sigma = 1.66$ and $\sigma = 1.59$) show a very similar level of TKE, whereas the highest driving pressure case ($\sigma = 1.53$) has significantly higher levels. This can perhaps be explained by the observations of L_{cav}^* from the high speed visualisation. The normalised cavity length for lower driving pressure cases were very similar, $L_{cav}^* = 0.13$ and $L_{cav}^* = 0.2$ respectively. Whereas the L_{cav}^* for the higher driving pressure case was significantly larger ($L_{cav}^* = 0.66$). This indicates that the TKE has a strong relationship with the distance from the cavity reattachment ($z/L - L_{cav}^*$) and is not as strongly linked to Reynolds number.

CONCLUSION

In order to understand the relationship between cavitation cavity length and turbulence in an axisymmetric large-scale nozzle, both high speed visualization and PIV measurements were conducted. High speed visualisation at 20,000 frames per second revealed the divergence of

the liquid jet upon exit of the nozzle depended strongly on the normalised cavity length, L_{cav}^* . Sequential frame analysis also revealed that for supercavitating conditions ($\sigma = 1.48$), shed bubble clouds have a significant influence on the structure of the spray resulting in rapid jet divergence and atomization directly from the nozzle exit. This was also shown to aid in the aerodynamic shear break-up mechanism and increase atomisation.

PIV measurements were taken for 3 cavitation numbers corresponding to the lowest 3 driving pressures, but were not possible for the supercavitation case due to laser reflections from the cavitation bubbles. Comparison of the relative increase in TKE energy to axial velocity demonstrated TKE to be highly dependent on the L_{cav}^* and less so on Re .

ACKNOWLEDGEMENTS

The authors would like to thank Mr Duncan Chalmers from the School of Mining Engineering for the generous use of his Photron high speed camera.

REFERENCES

1. Bergwerk, W., "Flow pattern in diesel nozzle spray holes". Proc Inst Mech Eng, 1959. 173: p. 655-660.
2. Reitz, R.D. and F.V. Bracco, "Mechanisms of atomization of a liquid jet". Phys. Fluids, 1982. 25(10): p. 1730-1742.
3. Soteriou, C., R. Andrews, and M. Smith, "Direct Injection Diesel Sprays and the Effect of Cavitation and Hydraulic Flip on Atomization". SAE, 1995. 950080.
4. Chaves, H., et al., "Experimental Study of Cavitation in the Nozzle Hole of Diesel Injectors using Transparent Nozzles". SAE, 1995. 950290.
5. Arcoumanis, C., et al., "Cavitation in Real-Size Multi-Hole Diesel Injector Nozzles". SAE, 2000. 2000-01-1249.
6. Kim, J., et al., "Characterization of Flows in the Sac Chamber and the Discharge Hole of a D.I. Diesel Injection Nozzle by Using a Transparent Model Nozzle". SAE, 1997. 972942.
7. Arcoumanis, C., et al., "Investigation of Cavitation in a Vertical Multi-Hole Injector". SAE, 1999. 1999-01-0524.
8. Ganippa, L.C., et al., "The Structure of Cavitation and its Effect on the Spray Pattern in a Single-Hole Diesel Nozzle". SAE, 2001. 2001-01-2008.
9. Brennon, C.E., "Cavitation and Bubble Dynamics". 1995: Oxford University Press.
10. Franc, J.P. and J.M. Michel, "Fundamentals of Cavitation". 2004: Springer.
11. Badock, C., et al., "Investigation of cavitation in real size diesel injection nozzles". International Journal of Heat and Fluid Flow, 1999. 20: p. 538-544.
12. Soteriou, C., R. Andrews, and M. Smith, "Further Studies of cavitation and Atomization in Diesel Injection". SAE, 1999. 1999-01-1486.
13. Sou, A., S. Hosokawa, and A. Tomiyama, "Effects of cavitation in a nozzle on liquid jet atomisation". International Journal of Heat and Mass Transfer, 2007. 50: p. 3575-3582.
14. Sou, A., S. Hosokawa, and A. Tomiyama, "Cavitation in a Two-Dimensional Nozzle and Liquid Jet Atomization". JSME International Journal, 2006. Series B, 49(4): p. 1253 -1259.
15. Ganippa, L., et al., "Cavitation: a contributory factor in the transition from symmetric to asymmetric jets in cross-flow nozzles". Experiments in Fluids, 2004. 36: p. 627-634.